

Prediction of performance of UHPFRC flexural member under blast loading

Rizwanullah, H.K. Sharma

Online Publication Date: 20 March 2023

URL: <http://www.jresm.org/archive/resm2023.633me0103.html>

DOI: <http://dx.doi.org/10.17515/resm2023.633me0103>

Journal Abbreviation: *Res. Eng. Struct. Mater.*

To cite this article

Rizwanullah, Sharma HK. Prediction of performance of UHPFRC flexural member under blast loading. *Res. Eng. Struct. Mater.*, 2023; 9(3): 921-946.

Disclaimer

All the opinions and statements expressed in the papers are on the responsibility of author(s) and are not to be regarded as those of the journal of Research on Engineering Structures and Materials (RESM) organization or related parties. The publishers make no warranty, explicit or implied, or make any representation with respect to the contents of any article will be complete or accurate or up to date. The accuracy of any instructions, equations, or other information should be independently verified. The publisher and related parties shall not be liable for any loss, actions, claims, proceedings, demand or costs or damages whatsoever or howsoever caused arising directly or indirectly in connection with use of the information given in the journal or related means.



Published articles are freely available to users under the terms of Creative Commons Attribution - NonCommercial 4.0 International Public License, as currently displayed at [here](http://creativecommons.org/licenses/by-nc/4.0/) (the "CC BY - NC").



Research Article

Prediction of performance of UHPFRC flexural member under blast loading

Rizwanullah*, a, H.K. Sharma^b

Department of Civil Engineering, National Institute of Technology, Kurukshetra, (Haryana) India

Article Info

Abstract

Article history:

Received 03 Jan 2023

Accepted 13 Mar 2023

Keywords:

*UHPFRC;
Spalling and Scabbing;
Damage behaviour;
Flexural member;
Total deformation*

An explosion within or near a building can cause terrible damage to the building. Ultra-high performance fibre reinforced concrete (UHPFRC) increases the strength and ductility of designing the structural elements with reduced sections. UHPFRC has a better load-carrying capacity, tensile strength (TS), and enhanced energy absorption capacity than the normal strength concrete (NSC) and high-performance concrete (HPC). This study focuses on understanding the behaviour of UHPFRC and HPC structural elements when subjected to the blast loading. Stress-strain behaviour, total deformation versus time response, and other ductility associated characteristics of UHPFRC based structural elements under blast loading of different charge weights were investigated. The design was carried out according to unified facilities criteria (UFC: 3-340-02). The total deformation of the beam was verified and compared with computed ANSYS R18.1 generated result. A significant reduction in total deformation was observed in UHPFRC compared to HPC and NSC structural elements. Flexural member designed to withstand a blast of 1.315 kN was found to resist a blast load of 5 kN within elastic range and up to 15 kN in the plastic field due to the inclusion of UHPFRC. The use of UHPFRC made the structural elements to reduced section dimensions thereby, decreasing the dead load, which is always advantageous in earthquake-resistant structures. UHPFRC can benefit blast-resistant facilities under high strain rates because of its extremely higher force capacity for the same size and reinforcement.

© 2023 MIM Research Group. All rights reserved.

1. Introduction

Structures under blast loading demonstrate improved strength than those subjected to static loading. The rapid strain rates in explosive-laden elements recognize the enhancement in force for composites and rebars [1]. The ultimate dynamic capacity is higher than its maximum static capacity. NSC and rebars are higher when subjected to high strain rates. HPC and UHPFRC illustrate higher compressive strength (CS), increased tensile resistance, toughness, and significant energy absorption capacity compared to NSC. UHPFRC and HPC are thus very economical to reduce the size of structural elements and develop resistance against blast loading [2].

Considerable significance has been given to blast loading effects on structures because of accidental or intentional activities due to terrorism. Therefore, it is imperative to protect civil infra-structures against blast shocks, accidental/deliberate actions worldwide target essential infrastructure facilities. There is a need to design the structures, especially of strategic importance, to withstand the effect of blast loads. Because of the nonlinear behaviour of material, dynamic response of the structure under blast loading is quite intricate and challenging to analyze. The progressive collapse of the structure is minimized by designing and constructing structural elements as blast-resistant. HPC has been found

*Corresponding author: rizwan_6170002@nitkkr.ac.in

^a orcid.org/0009-0000-4145-5798; ^b orcid.org/0000-0001-7713-1998

DOI: <http://dx.doi.org/10.17515/resm2023.633me0103>

Res. Eng. Struct. Mat. Vol. 9 Iss. 3 (2023) 921-946

to impart more strength, durability, and serviceability on this front to obtain reduced section dimensions of the features. An extensive literature review study reveals that HPC has a better ability to load carrying capacity, TS, and significant energy absorption capacity than NSC. This study concentrates on enhancing the understanding of behaviour of UHPFRC and HPC structural elements under blast loading.

2. HPC and UHPFRC

The term high performance infers an improved arrangement of structural properties like durability, stiffness, strength, energy absorption capacity, multiple cracking, etc., considering the overall cost of the material and the products manufactured. HPC is defined as concrete with superior performance and uniformity that can be accomplished using special mixing, placing, and curing techniques. The structure involves high early strength, long-term mechanical properties, durability and toughness, longer life under poor environmental conditions, flowability, and self-leveling capacity. It also has a high modulus of elasticity, low permeability, placement, and compaction without segregation and resistance to chemical attack [3]. HPC is manufactured with high-quality material ingredients and a proper mix design. It has a low water-binder ratio and excellent performance characteristics that satisfy the requirements to withstand high tensile and flexural stresses subjected to high-intensity blast loads. UHPFRC is another novel material class with exceptionally high strength and durability. It is high in strength and flexibility and is prepared by mixing cement, fine silica sand, silica fume, quartz floor, plasticizer, high-strength steel fibres (SF), and water [4].

UHPFRC, a new class of material, which was developed to overcome the comparatively brittle behaviour of HPC. Larrard FD et al. [5] presented the term UHPFRC, which required hot curing at 90° C or higher and vacuum pressure before and during the setting. Although these special procedures are advantageous to mechanical properties, they result in high-energy consumption and low production efficiency [6]. Therefore, researchers have conducted a good selection of materials to influence the mechanical and microstructural properties and durability of UHPFRC to facilitate its production and application. The typical static stress-strain behaviour of UHPFRC in compression is illustrated in Fig. 1.

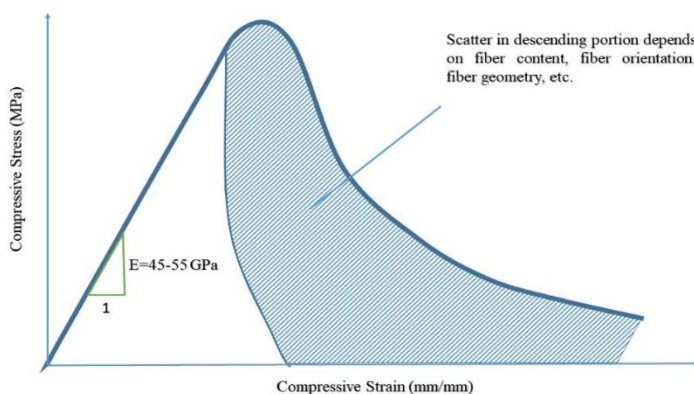


Fig. 1 Compressive stress-strain curve of UHPFRC [7]

The behaviour of UHPFRC is characterized by very high CS, more than 150 MPa, elastic modulus, TS of 4-5 % of CS, and a significantly higher post-peak ductility. Generally, the influence of SF on enhancing CS and elastic modulus is very low [8]. UHPFRC is expensive compared to NSC and requires hot curing, and the mix must be designed appropriately to

suit unique structures. The TS of UHPFRC varies from 8 to 15 MPa [9], as illustrated in Fig. 2. The tensile behaviour of UHPFRC is characterized by linear-elastic stress level corresponding to TS, strain hardening behaviour corresponding to non-continuous micro-cracks in the cementitious paste ended by single crack localization. After that, the resistance drops, and strain-softening behaviour is exhibited until complete failure. SFs strongly affect the stress-strain curve's behaviour and post-cracking non-linear descending portion.

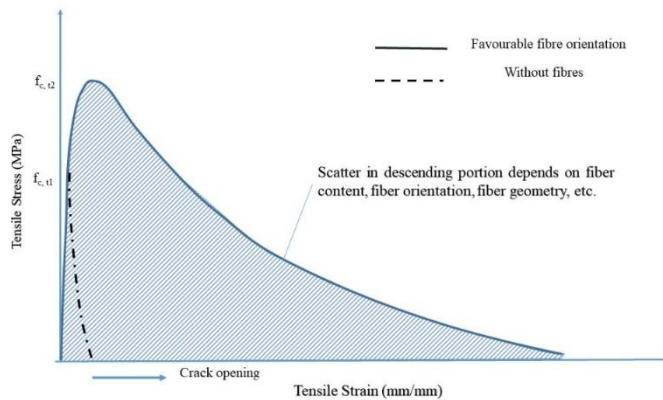


Fig. 2 Tensile behaviour of UHPFRC [7]

Structural performance assessment against blast loading is an urgent issue that needs to be addressed due to increased terrorist activities and unintentional explosions. Computer modeling involving numerical analysis is considered valuable for modeling such structures when subjected to blast loading. Therefore, the current study is intended to investigate the response of NSC, HPC, and UHPFRC structural elements using UFC 3-340-02 to explore HPC and UHPFRC structural elements using standard software ANSYS R18.1 for other blast loading conditions.

3. Explosion and Blast

The blast effect of an explosion is in the form of shock waves comprising of a high intensity shock wave front that develops outward from the surface of explosive into the adjacent air. As the wave propagates, it decays in strength, lengthens in duration, and decreases in velocity. This phenomenon is created by spherical deviation and chemical reactions, but for some after-burning related with the hot explosion products mixing with the nearby surrounding. As the wave develops in the air, the front impinges on constructions within its path, and shock pressures engulf the whole system. The magnitude and dispersal of the blast loads arising from these pressures are a function of the factors like explosive characteristics (lower or higher order detonation) and explosive weight, the location of the explosion, and magnitude of the reinforcement. The blast loading on the structures can be classed into two categories on the basis of confinement of the systems, confined explosion, and unconfined explosion [10].

3.1 Pressure and Time Profile of Blast Load

The blast pressure vs. time profile is illustrated in Fig. 3. At an arrival time t_A due to explosion, the pressure increases suddenly to a peak overpressure, P_{so} , on ambient pressure (P_o). Then, pressure decreases to the ambient level at a time t_o decrease again to an under-pressure P_{so^-} until ambient conditions are attained. The term P_{so} is denoted as

peak overpressure, incident peak overpressure, or peak overpressure. The incident peak overpressure P_{so} is augmented by a reflection factor as the shock wave comes across the structure in its path. The reflection factors, which are affected by shock wave intensity and normal incidence in the case of explosives, can raise incident pressures by an order of magnitude. Two main phases are observed during the pressure-time profile. The portion above ambient is called +ve phase of duration, denoted by t_o , and the leg below ambient is -ve phase of time, t_o^- . The -ve phase is always has a longer but lower intensity than the +ve duration. When standoff distance (SD) increases, positive-phase blast wave duration also increases, leading to a longer-duration shock pulse of lower amplitude. Blast charges close to a target inflict an impulsive and high-intensity pressure load, whereas blast charges at some distance yield a low intensity- longer-duration uniform pressure of lower intensity over the structure. Finally, in this process, the whole target is bounded by the shock wave, with diffraction and reflection effects forming shadow and focused zones around the structure. The deteriorated structure can be subjected to fragments, which may cause further destruction during the -ve phase. The ambient pressure increases and subsequently decreases forming a triangular overpressure. Brode [11] obtained peak overpressure expressions in close-in-contact conditions.

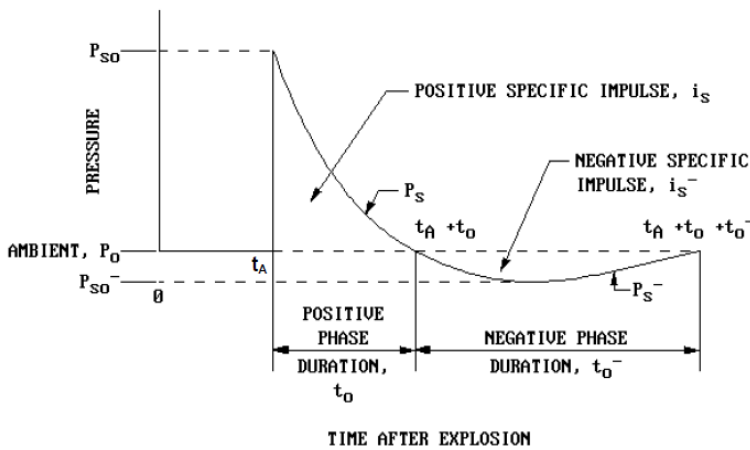


Fig. 3 Pressure vs. time profile [10]

It is crucial that the negative pressure phase marks in a vacuum in which air gets filled accordingly at a faster rate, on account of which pressure acts in a direction reverse top to the incident pressure. Therefore, just like seismic loads, blast loads are also cyclic. However, the number of cycles and frequency is inconsequential compared to the positive one. The negative amplitude, almost negligible compared to the P_o negative phase, is often neglected to simplify the analysis. Baker recommended Friedlander's equation (12) as,

$$P_s(t) = P_{so} \left(1 - \frac{t}{t_o}\right) e^{-b \frac{t}{t_o}} \tag{1}$$

Here 'P (t)' represents the incident pressure at (t), '(P_o)' is the region atmospheric pressure, '(P_{so+})' is peak positive incident over-pressure, and '(t_{pos})' is positive phase duration. The decay parameter is (b). The integrated area under the pressure history curve is called impulse. The impulse is called a positive specific impulse for the positive pressure phase, and for the negative pressure phase, it is called a negative specific impulse. Fig. 4 illustrates various strain rate values for different extreme load scenarios. The strain rate ranges in 10^{-8} s^{-1} are considered for creep and 10^3 s^{-1} for explosive loading (blast and impact loads).

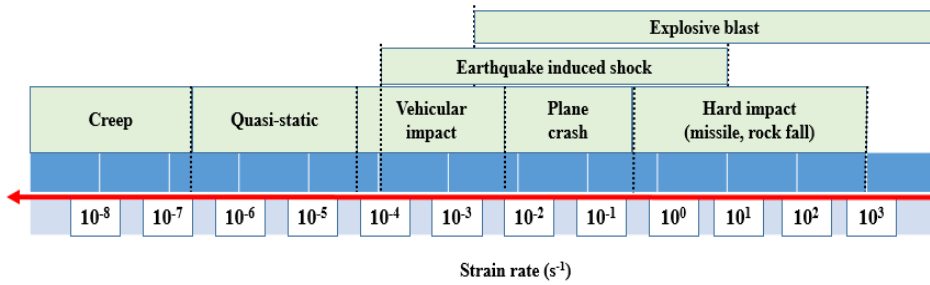


Fig. 4. Ranges of Strain rate for Concrete Structures [9]

3.2 Prediction of the Blast Wave

Many researchers also provided empirical equations for overpressures ' P_{so} ' in units of MPa, weight of charge ' w ' in kg, ' R ' is the SD in meters, and scaled distance, $[Z = \frac{R}{W^{\frac{1}{3}}}]$ in $m / (kg^{1/3})$ as tabulated in Table 1.

Table 1. Empirical equations anticipated by different authors for peak positive overpressure ' P_{so} '

S.No	Author (s)/ year	Equations
1.	Sadovskyi (1952) [13]	$P_{so} = \frac{0.085}{Z} + \frac{0.3}{Z^2} + \frac{0.82}{Z^3}$
2.	Brode (1955) [11]	$P_{so} = \frac{0.0975}{Z} + \frac{0.1445}{Z^2} + \frac{0.585}{Z^3} - 0.0019$ for $(0.01 \leq P_{so} \leq 1)$ $P_{so} = \frac{0.67}{Z^3} + 0.1$ for $(P_{so} > 1)$
3.	Adushkin and Korotkov (1961) [14]	$P_{so} = \frac{0.08}{Z} + \frac{0.28}{Z^2} - \frac{0.322}{Z^3}$
4.	Newmark and Hansen (1961) [15]	$P_{so} = 93 \left(\frac{W}{R^3}\right)^{\frac{1}{2}} + 6784 \frac{W}{R^3}$
5.	Henrych and Major (1979) [16]	$P_{so} = \begin{cases} \frac{14.072}{Z} + \frac{5.54}{Z^2} - \frac{0.375}{Z^3} + \frac{0.00625}{Z^4} & \text{for } (0.05 < Z < 0.3) \\ \frac{-6.194}{Z} - \frac{0.326}{Z^2} + \frac{2.132}{Z^3} & \text{for } (0.3 \leq Z \leq 1) \\ \frac{0.662}{Z} + \frac{4.05}{Z^2} + \frac{3.288}{Z^3} & \text{for } (1 \leq Z \leq 0.3) \end{cases}$
6.	Held (1983) [17]	$P_{so} = 2 \frac{W^{\frac{2}{3}}}{R^2}$

7.	Kinney and Graham (1985) [18]	$P_{so} = P_0 \cdot \frac{808 \left[1 + \left(\frac{Z}{4.5} \right)^2 \right]}{\left\{ \left[1 + \left(\frac{Z}{0.048} \right)^2 \right] \times \left[1 + \left(\frac{Z}{0.32} \right)^2 \right] \times \left[1 + \left(\frac{Z}{1.35} \right)^2 \right] \right\}^{\frac{1}{2}}}$
8.	Mills (1987) [19]	$P_{so} = \frac{0.108}{Z} - \frac{0.114}{Z^2} + \frac{1.772}{Z^3}$
9.	Hopkins-Brown and Bailey (1998) [20]	$P_{so} = \begin{cases} -1.245 + \frac{1.935}{Z} + \frac{0.2353}{Z^2} - \frac{0.01065}{Z^3} & \text{for } (0.05 \leq Z \leq 1.15) \\ \frac{0.0707}{Z} + \frac{0.3602}{Z^2} + \frac{0.4891}{Z^3} & \text{for } (1.15 < Z \leq 40) \end{cases}$
10.	Low and Hao (2001) [21]	$P_{so} = \begin{cases} \frac{1.050}{Z^3} - 0.0981 & \text{for } (Z \leq 1) \\ \frac{0.0745}{Z} + \frac{0.250}{Z^2} + \frac{0.637}{Z^3} & \text{for } (1 < Z \leq 15) \end{cases}$
11.	Gelfand and Silnikov (2004) [22]	$P_{so} = \begin{cases} 1.7 \times 10^3 \exp(-7.5 \times Z^{0.28}) + 0.0156 & \text{for } (0.1 \leq Z < 8) \\ 8 \times 10^3 \exp(-10.7 \times Z^{0.1}) & \text{for } (Z \geq 8) \end{cases}$
12.	Wu and Hao (2005) [23]	$P_{so} = 1.059 \times Z^{-2.56} - 0.051 \quad \text{for } (0.1 \leq Z \leq 1)$ $P_{so} = 1.008 \times Z^{-2.01} \quad \text{for } (1 < Z \leq 10)$

3.3 Structural Response with Blast Loading

The structure's behaviour under blast is usually denoted in design ranges in the form of pressure intensity as high, low, and very low, Fig. 5. At the high-pressure design zone, curve A, the duration of the load applied is short, mainly when venting of the explosion product of the detonation happens. The durations are lacking compared to the response- time of the individual elements of the structures. In the case of the low-pressure design of curve B, structures under blast pressures withstand smaller peak pressures than those related with an earlier range corresponding to curve A. Structural elements are therefore designed for the low-pressure range depending on impulse and pressure. Likewise, in the case of a very low-pressure design range, curve C, blast pressure duration is substantial compared to the response time. The structure responses designed to withstand the impact of detonations are considered in the "very low-pressure range."

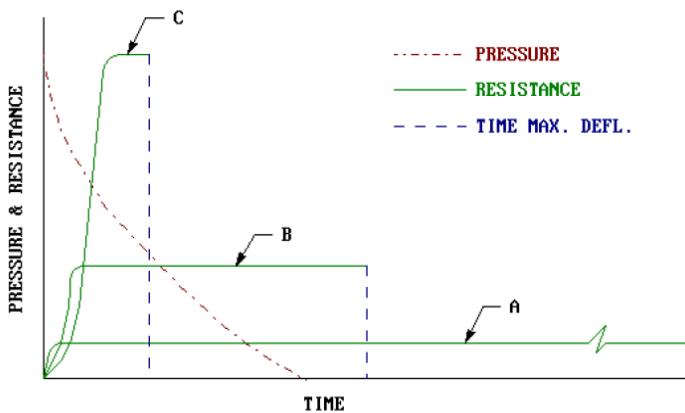


Fig. 5. Variation of structural response and blast load vs. time [24]

4. Published Literature

Luccioni, BM et al. 2004 [25] studied the failure of RC buildings caused by blast loading and validated the damage produced after the explosion. They concluded that the numerical results showed collapse under the blast load. The failure was due to the destruction of lower columns. Byfield, MP et al. 2006 [26] studied the behaviour of blast loading on structures. In recent attack happened due to the detonation of vehicle-borne devices in the Middle East, Europe, and North America. Modern commercial buildings may be vulnerable to progressive collapse, as seen during the attack on the Murrah building in 1995. Conventional beams showed a noteworthy higher flexural strength during design. Vehicle-used devices were capable of destroying the frame system at close range. Ngo, T et al. 2007 [1] extensively studied the influence of blasts on the structure. Terrorist organizations have used vehicle bombs to assault worldwide in their activities. A bomb explosion inside or nearby can inflict major damage to the structures' internal and external frames, collapse walls, window panels, and cause the loss of humans. The structural analysis and design under blast loading necessitate a deep knowledge of diverse structures' dynamic responses and blast phenomena. Yanchao, S et al. 2007 [27] conducted numerical simulations to investigate the blast wave interaction in a structural column. It was observed that when the blast wave column behaviour is considered, the influence marginally decreases the positive reflected pressure and the positive impulse increases. They concluded that the blast column interaction is significantly influenced by column size. UFC 3-340-02, 2008 [10] illustrated the step-to-step analysis and design methods. The parameters included the dynamic analysis, blast fragment, reinforced concrete (RC), and steel construction shocks. Zeynep, K et al. 2008 [28] observed a rise in the terrorist attack, and the effects of blast loading on the structure is a great concern that should be considered in the construction and design. The attacks were artificial and dynamic blast loads that were calculated similarly to wind and earthquake loads. The buildings protect to resist blast load using several techniques in structural design. Every member of the structure should be designed to stand blast load. Nystrom, U et al. 2009 [24] conducted an analytical investigation to study the influence of fragments caused by explosions. The combined blast and fragment loading effects on RC walls were investigated using a numerical simulation. Numerical simulations were conducted on the response subjected to fragments and blast loading. Wu, C et al. 2009 [29] investigated a series of test conducted on slabs under blast loading. Different types of slabs were cast and tested using UHPFRC, reinforced ultra-high performance fibre concrete (RUHPFC), and fibre reinforced polymer (FRP). The authors concluded that the UHPFRC slabs suffered less damage as compared with RC slabs when subjected to blast loading. Hassan, MZ et al. 2012 [30] investigated blast resistance of sandwich panels made up of aluminium alloy. Experimental studies were carried out using a ballistic pendulum, and it was found that the sandwich panels were damaged as the density of foam increased. The authors also concluded that the blast response of sandwich structures showed significant energy absorption. Shallan, O et al. 2014 [31] investigated the influence of blast loading on buildings for different ratios numerically. Finite element simulation on the buildings was developed using AUTODYN. Blast loads with varied SDs were applied at two distinct locations and distanced from the structure. Nicolaides, D et al. 2015 [32] studied the mechanical and fracture behaviour of UHPFRC under blast loading. The mix's water-to-binder ratio and SFs were 0.16 as 6%, respectively. The authors concluded that the CS and fracture energy obtained were obtained as 175 MPa and 26000 N/m, respectively. Conrad K et al. 2017 [33] presented the influence of axial loading and transverse reinforcement spacing on RC columns at a small-scaled distance under blast loading. An analytical study was conducted to understand the transverse reinforcement effects under blast loading on RC columns. Li et al. 2017 [34] investigated the blast resistance of segmental RC columns. The results indicated that the performance of RC columns under blast loading differs from seismic excitation on the ground. The author

performed a numerical analysis of RC columns segmentally. The central deflection of the segmental column under blast load is reduced by the addition of prestress by post-tensioning tendons. The results showed that the behaviour of segmental columns subjected to blast loading differs from that of seismic ground excitations. Yang, HW et al. 2018 [35] studied the failure behaviour of four different hemispherical shells subjected to blast loading. Simulation studies of the collapse behaviour of hemispherical shells were conducted using ANSYS and LS-DYNA. The analysis considered material and geometric non-linearities for extreme loading conditions. Experiments and computations demonstrated relatively small variation for both empty and liquid-filled shells. Kaan, T et al. 2019 [36] studied the flexural behaviour of UHPFRC beams numerically and experimentally. The fibre used in the beam is 13 mm straight fibre and 60 mm hooked fibre. The deflection of non-fibre beams varies from 8.14 to 2.11 while increasing the reinforcement ratio. Rizwanullah et al. 2020 [2] presented an extensive review to study the effect of various parameters on UHPFRC elements under blast loading. They also discussed the effects of w , blast loading with changing CS, and SD. It was observed that detailing structural elements under earthquake conditions also presents improved blast performance.

An extensive literature review conducted to study the influence of blast loading illustrated that several investigators had studied the effect of blast intensity, SD, and location of the blast in their studies. However, researchers did not consider the influence of elevated temperature on structural elements. Lee, J-Y et al. 2020 [37] investigated six RC columns of $160 \times 160 \times 2468$ mm and tested them using a shock tube. In addition to retrofitted jackets, UHPFRC was studied to calculate the influence of seismic detailing and transverse reinforcement. UHPFRC columns were improved by including seismic in the case of blast and impact resistance. Castedo, R et al. 2021 [38] investigated RC slabs under close-in explosion. The slab was subjected to 1.74 kg of trinitrotoluene (TNT) at 1 m and the other slab of 13.05 kilograms of TNT at 0.5 m.

Scaled distance determines the type of failure and damaged concrete slab area. Khadim, MMA et al. 2021 [39] studied the performance of UHPC in comparison to NSC. UHPC has exceptional CS and carries less post-cracking tensile behaviour. The beams with and without fibres were modeled in finite element analysis (FEA) and validated results with a reinforcement ratio of 0.009. Mahmud, GH et al. 2021 [40] investigated the structural behaviour of UHPFRC under bending. They have performed using different thickness and boundary conditions, i.e., simply supported and fixed ends. The failure pattern in both conditions has similar cracks. Further, very few analytical works have been done on the behaviour of HPC and UHPFRC structural elements under close-range blast conditions. No one has recommended analysis and design procedures for structural components to resist different blast loading. Mandal, J et al. 2021 [41] studied the post-blast release of kinetic energy, and some were converted into ground shock waves, which affect the shock propagation and crater depth. The present study has therefore been conducted to investigate these parameters. Anas, SM et al. 2022 [42] investigated RC structures used to store ammunition, explosives, and chemical weapons. Such structures are considered very important, like war zones under critical conditions. The structures were subjected to extreme loading conditions from blasts and explosions. Safe on-ground, free air SDs, and safe blast pressure, were forecast for both the hemispherical surface detonation (HSD) and spherical air detonation (SAD). It was concluded that the proposed shelter can withstand blast loads of 4.98 and 0.93 MPa against SAD and HSD, respectively. Yan, J et al. 2022 [43] investigated the combination of UHPC with Glass fibre reinforced concrete (GFRP) structure subjected to blast loading. The authors studied damage caused by UHPC beams for different scaled distances. Adding GFRP in the beams improves the blast resistance of UHPC compared with NSC. LL, M et al. 2023 [44] investigated critical infrastructures prone

to accidental and manmade explosions. The authors analytically evaluate the performance of RC beams/columns subjected to blast loading. The researchers concluded that the scaled distance for global and local responses of RC members can be determined as $0.78 \text{ m/kg}^{1/3}$.

Calculation of peak overpressure using UFC 3-340-02 [10]

Calculation of blast parameters for 5 kN of TNT.

Steps:

1. Given data,
Height (H_c) = 10m = 32.8 ft., Length (L) = 10m = 32.8 ft.
Weight = 5 kN = 1102.31 lbs.
2. Apply a 20% safety factor to the charge weight
 $W = 1.2 (1102.31) = 1322.772 \text{ lbs.}$
3. At the point of interest, evaluate the SD, 'R', and 'Z'

$$R = \sqrt{(32.8)^2 + (32.8)^2} = 46.4 \text{ ft.}$$

$$Z = \frac{R}{W^{1/3}} = \frac{46.4}{(1322.772)^{1/3}} = 4.2 \text{ ft/lb}^{1/3}$$

4. Determine incident blast wave parameters, see Fig. (6-7)

$$P_{so} = 50 \text{ psi}$$

Positive incident impulse, ' i_s '

$$\frac{i_s}{W^{1/3}} = 35 \text{ psi-ms/lb}^{1/3}$$

$$i_s = 35 (1322.772)^{1/3} = 384.2 \text{ psi-ms}$$

Positive phase duration, t_o

$$\frac{t_o}{W^{1/3}} = 1.5 \text{ ms/lb}^{1/3}$$

$$t_o = 1.5 (1322.772)^{1/3} = 16.46 \text{ ms}$$

Arrival time, t_A

$$\frac{t_A}{W^{1/3}} = 0.9 \text{ ms/lb}^{1/3}$$

$$t_A = 0.9 (1322.772)^{1/3} = 9.88 \text{ ms}$$

For negative blast wave pressure,

Negative incident pressure, $P_{so}^- = 3 \text{ psi}$

Negative phase duration, t_o^-

$$\frac{t_o^-}{W^{1/3}} = 8 \text{ ms/lb}^{1/3}$$

$$t_o^- = 8 (1322.772)^{1/3} = 87.82 \text{ ms}$$

Positive and negative blast wave parameters and Peak overpressure for positive phase time for different TNT charge weights are tabulated in Table 2. Fig. (6-7) represent as negative and positive phase duration of free air explosion.

Table 2. Peak overpressure and time for different charge weight

Load (kN)	Peak Overpressure (MPa)	Positive Phase				Negative Phase	
		P_{so} (psi)	i_s (psi-ms)	t_o (ms)	t_A (ms)	P_{so}^- (psi)	t_o^- (ms)
5	0.344	50	384.2	16.46	9.88	3	87.82
10	0.55	80	221.3	19.63	9.68	4	99.57
15	0.655	95	269.14	23.74	7.6	7	118.7
25	1.103	160	375.41	28.16	7.5	9	140.8

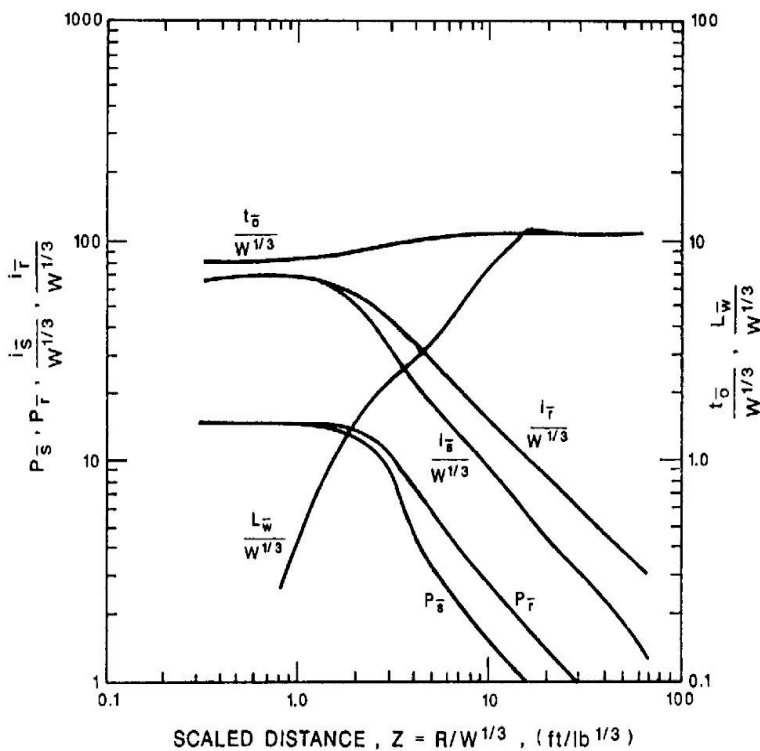


Fig. 6 Negative Phase Parameter of Free Air Explosion [10]

An interior roof slab-beam assembly has studied the behaviour of flexural members for free air blast loading shown in Fig. 8. The assembly section was analyzed and designed by UFC 3-340-02 for NSC, HPC, and UHPFRC. Free airbursts of charge weights 1.315, 5, 10, 15, and 25 kN TNT were considered for evaluating the blast wave parameters. The detonation was assumed at 10 m above the ground and 10 m away from the point of interest. An intermediate T- beam was considered for HPC and UHPFRC under blast loading from UFC 3-340-02. A free airburst was assumed to occur, and negative phase pressure was neglected due to the very low intensity of the blast. The equivalent elastic deflection, X_E

was obtained as 1.27 mm. For the natural period of the beam corresponding to 16.77 ms, blast wave parameters were calculated for different TNT charges.

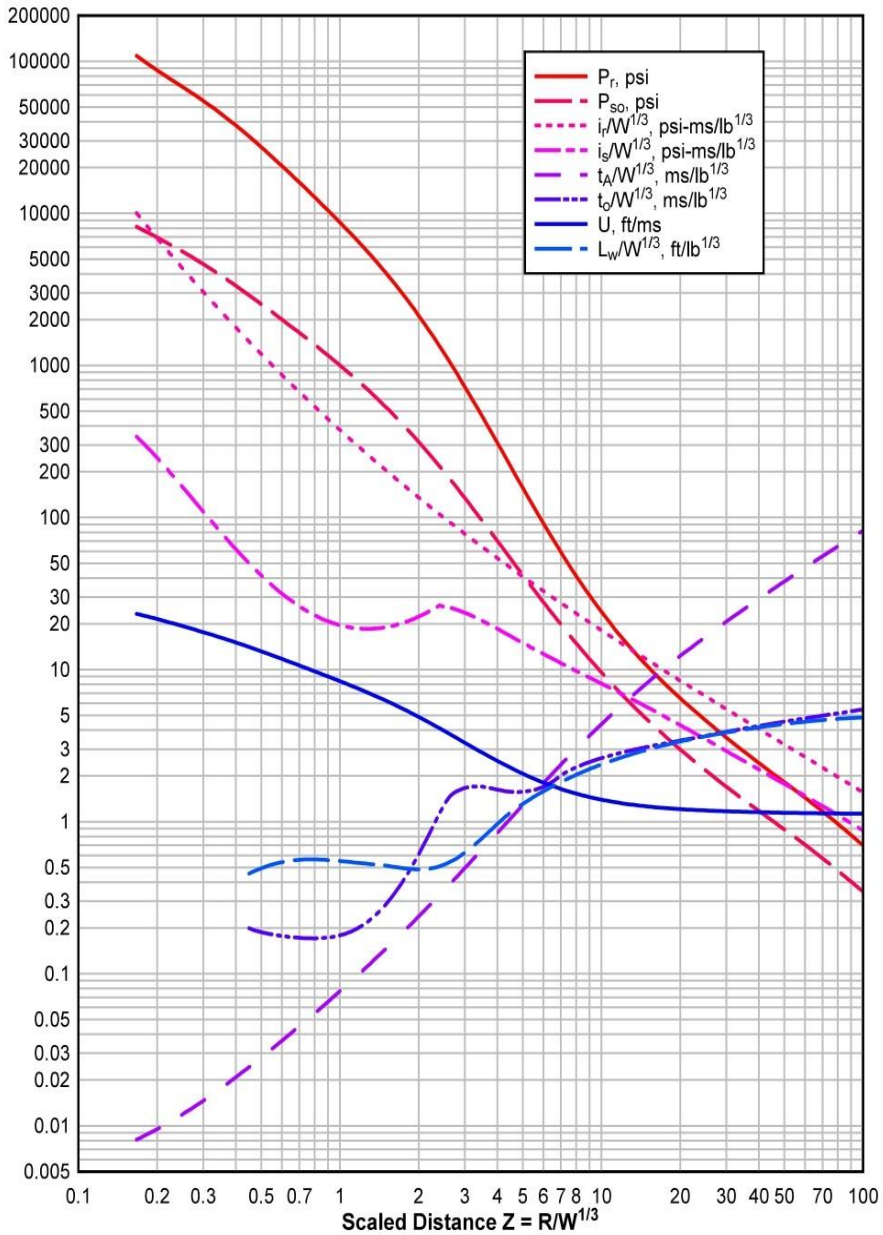


Fig. 7 Positive Phase Parameter of Free Air Explosion [10]

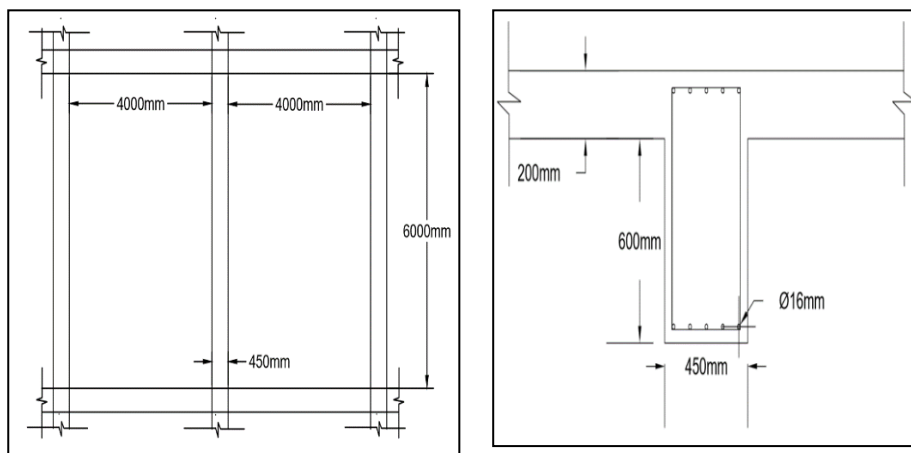


Fig. 8 Plan of an interior roof beam and section of Interior roof T- beam

5. Analytical Investigations

A finite element analysis using standard software ANSYS R18.1 was conducted to validate the typical results obtained. 3D solid elements SOLID 65 and LINK8 were used for nonlinear modeling of concrete and reinforcement for numerical simulation, as shown in Fig. 9. When cracking and concrete crushing are used, the load is gradually applied to check the possible crushing of concrete before proper load transfer takes place through a closed crack.

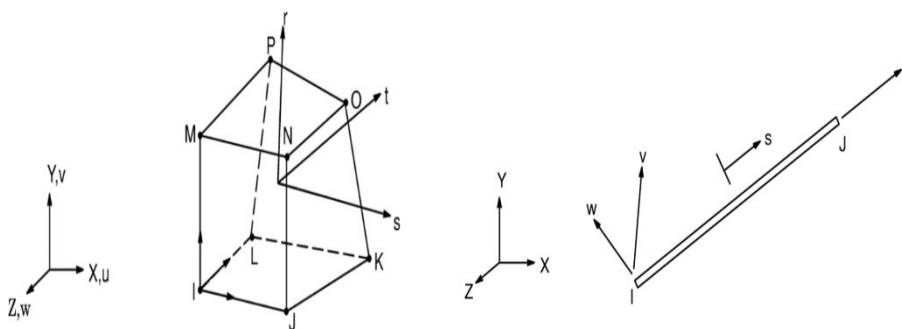


Fig. 9 Solid 65 and Link 8 Element [45]

5.1 Modelling of Interior Roof Slab Beam Assembly

Modeling the flexural member assembly was done in ANSYS R18.1 explicit dynamic software, Fig. 10. The geometry of the beam has been made in the Design Modular of explicit dynamics. The body interaction in explicit dynamics automatically made the bonded connection between steel reinforcement and concrete. UFC 3-340-02 calculates the end time of the analysis in the positive phase duration of the pressure of different blast loading conditions. Table 3 illustrates the properties of steel reinforcement and concrete for NSC, HPC, and UHPFRC, respectively.

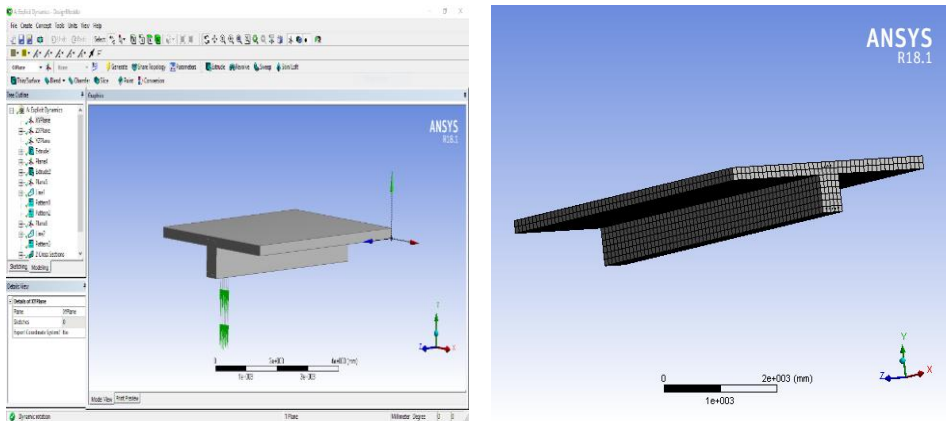


Fig. 10. Design Modular user interface of the software and meshed of interior roof

Table 3. Properties of the material

Steel Reinforcement Properties		RHT Concrete Model of NSC, HPC, and UHPFRC			
Properties/Unit	Values	Properties/Unit	Values		
Density (kN/m ³)	78.50	NSC	HPC	UHPFRC	
Young's Modulus (MPa)	200000	Density (kN/m ³)	23.14	24.00	25.00
Poisson's ratio	0.3	Specific heat (J/Kg °C)	654	654	654
Bulk Modulus (MPa)	166670	CS, f_c (MPa)	35	80	140
Shear Modulus (MPa)	76923	TS, f_t/f_c	0.1	0.15	0.2
Tensile Yield Strength (MPa)	415	Shear strength, f_s/f_c	0.18	0.2	0.28
Specific Heat (J kg ⁻¹ C ⁻¹)	434	Compressive strain rate exponent, α	0.032	0.0091	0.0091
Plastic Failure Strain	0.02	Tensile strain rate expo, δ	0.036	0.00125	0.0013
Strain-Life Parameters		Minimum strain to failure	0.01	0.01	0.01
Strength Coefficient	920	Damage constant, D_1	0.04	0.04	0.04
Strength Exponent	-0.106	Damage constant, D_2	1	1	1
Ductility Coefficient	0.213	Shear modulus (MPa)	16670	22060	22060

Cyclic Hardening Coefficient	Strain 0.2	Solid density (kN/m ³)	27.50	27.50	27.50
Porous sound speed (m/sec)			2920	3242	3242
Initial compaction pressure, P _e (MPa)			23.3	93.3	93.3
Solid compaction pressure, P _s (MPa)			6×10 ³	6×10 ³	6×10 ³
Compaction exponent, n			3	3	3

ANSYS R18.1 software was used for explicit dynamics for finite element modeling to solve time-dependent load problems. Explicit dynamics divide the problem into four categories: engineering data, geometry, model, and results. The geometry is part of the solver in which the problem has been to be taken. Explicit dynamics used the Design Modeler program to draw the geometry. In the model part of explicit dynamics, various steps are connections, meshing, analysis settings, pressure application, support fixing, and the results. Explicit dynamics automatically make connections between two different materials depending on their properties.

6. Analysis and Discussion of Results

The analytical investigation on NSC, HPC, and UHPFRC structural elements was conducted under blast loading using ANSYS R18.1 software. The characteristic CS of NSC, HPC, and UHPFRC for 35, 80, and 140 MPa, respectively, for TNT charge 5, 10, 15, and 25 kN. This paper has studied the flexural members of different magnitudes at 10 m above and away from the structures. The assembly was designed to resist an airburst of charges of 1.315 kN. The deflection corresponding to equivalent elastic deflection and maximum deflection for such a control beam (CB) has been calculated as 1.27 mm and 19.75 mm, respectively.

6.1 Stress-Strain Behaviour

The typical results of stress-strain behaviour for NSC, HPC, and UHPFRC beams for TNT charge corresponding to 5, 10, 15, and 25 kN are illustrated in Fig. 11-12, respectively. It has been observed that for a TNT charge of 5 kN, values of maximum stress have been obtained as 49.22, 48.53, and 51.57 MPa in NSC, HPC, and UHPFRC beams, respectively, whereas values of maximum strain are obtained as 0.001137, 0.001618, and 0.00026 mm/mm, in the corresponding beams. It was also found that there is no substantial change in maximum stress values corresponding to NSC and HPC beams. However, HPC beams illustrated a significant increase in elastic deformation by 142%. HPC is, therefore, found to behave more elastically than NSC. There was an increase in maximum stress value in UHPFRC in the beam, but the max strain was significantly decreased, illustrating no damage in the UHPFRC beam for a blast of 5 kN TNT. UHPFRC beam remained intact without any damage. It is also stated that stress-strain behaviour has only been plotted for ascending values for the first cycle. This trend was observed in several processes until stresses and strains were finally stabilized. An identical behaviour was observed in the case of 10 and 15 kN of TNT charges. However, in the case of the 25 kN TNT charge, the maximum strain value is significantly on the lower side, illustrating that UHPFRC, being of high strength and stiffness, behaved linearly during 25 kN of TNT.

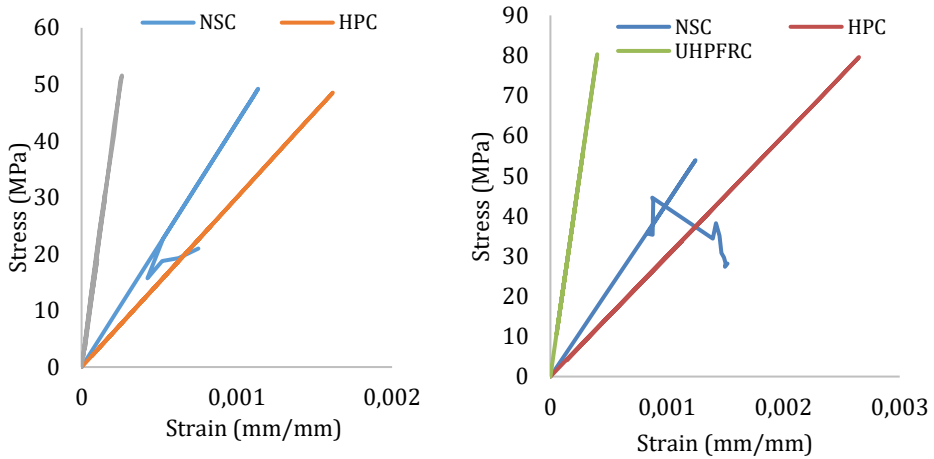


Fig. 11 Stress-Strain behaviour of NSC, HPC, and UHPFRC beams for 5 and 10 kN of TNT

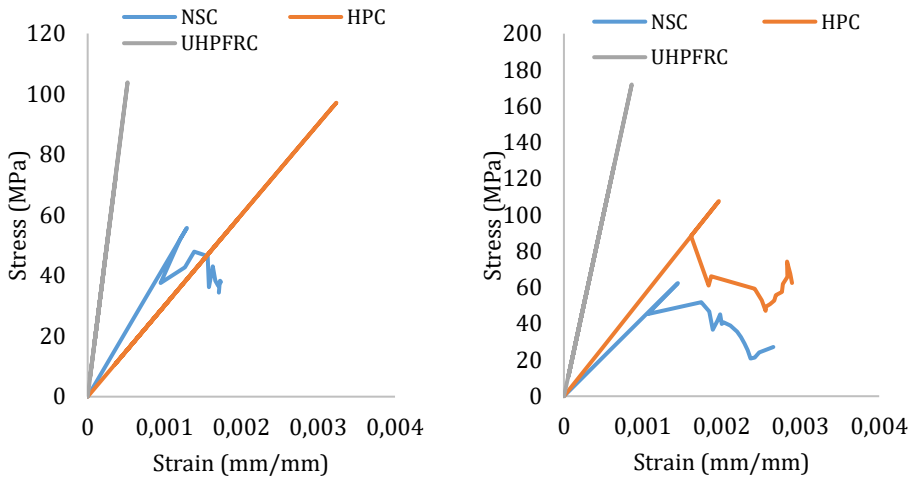


Fig.12 Stress-Strain behaviour of NSC, HPC, and UHPFRC beams for 15 and 25kN of TNT

6.2 Total Deformation-Time Behaviour

The variation of total deformation with time regarding NSC, HPC, and UHPFRC beams for TNT charge corresponding to 5, 10, 15, and 25 kN are shown in Fig. 13-14, respectively. It was found that there is a significant decrease in maximum values corresponding to NSC and HPC beams. UHPFRC beams illustrated a substantial reduction in total deformation to 0.89 mm compared to 6.89 and 5.53 mm in the case of the control beam of NSC and HPC beam for a TNT of 5 kN. UHPFRC is therefore found to illustrate significant ductility than NSC and HPC. There was a decrease in deformation value in the UHPFRC beam while demonstrating no damage in the UHPFRC beam for a blast of 5 kN TNT. UHPFRC beam remained intact without any damage. Maximum stress-strain behaviour and total deflection values of NSC, HPC, and UHPFRC are obtained at different times in these composites, as shown in Table 4. A significant reduction in total deformation was observed

in the case of HPC and UHPFRC beams compared to the control beam of NSC, clearly illustrating that HPC and UHPFRC showed tremendous resistance to blast loading compared to the NSC beam.

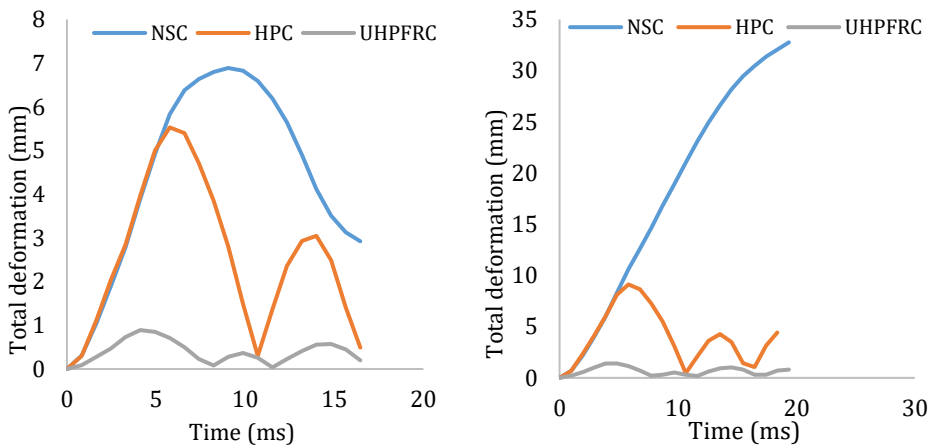


Fig.13 Total deformation and time graph of NSC, HPC, and UHPFRC for 5 and 10 kN of TNT

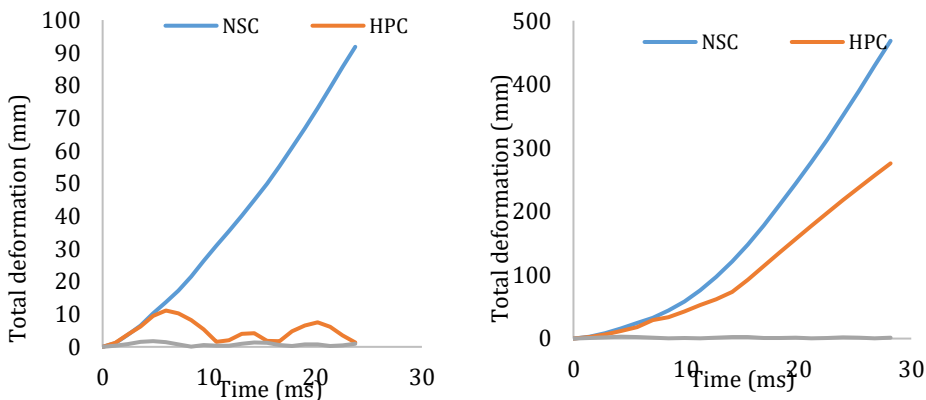


Fig.14 Total deformation and Time Graph of NSC, HPC, and UHPFRC for 15 and 25 kN of TNT

Table 4. Maximum Stress-Strain and deformation values with time for NSC, HPC, and UHPFRC

Blast Load, TNT (kN)	Time (ms)	Maximum Stress-Strain						Time (ms)	Total deformation (mm)		
		NSC		HPC		UHPFRC			NSC	HPC	UHPFRC
		Stress (MPa)	Strain (mm/mm)	Stress (MPa)	Strain (mm/mm)	Stress (MPa)	Strain (mm/mm)				
5	8.23	49.22	0.001137	-	-	-	-	9.06	6.89	-	-
	6.59	-	-	48.53	0.001603	-	-	5.77	-	5.53	-
	4.95	-	-	-	-	51.57	0.00021	4.12	-	-	0.89
10	5.81	53.92	0.001246	-	-	-	-	19.37	32.77	-	-
	5.81	-	-	79.61	0.00265	-	-	5.81	-	9.13	-

	3.88	-	-	-	-	80.31	0.0040 2	4.84	-	-	1.41
15	4.75	55.76	0.001289	-	-	-	-	23.7 4	91.8	-	-
	5.94	-	-	97.11	0.03237	-	-	5.94	-	11.11	-
	4.75	-	-	-	-	103.8 5	0.0005 2	4.75	-	-	1.74
25	4.22	62.38	0.00144	-	-	-	-	23.9 4	350.9	-	-
	4.22	-	-	107.61	0.00197	-	-	28.1 6	-	275.5 7	-
	4.22	-	-	-	-	171.9 5	0.0008 6	4.23	-	-	2.99

6.3 Equivalent Stress and Equivalent Strain Pattern

Free air explosion on flexural members was analyzed to study the equivalent stress behaviour for NSC, HPC, and UHPFRC beams under TNT charge corresponding to 5, 10, 15, and 25 kN. The worst situation is in the NSC, HPC, and UHPFRC beam under 25 kN TNT. Fig. 15-20 illustrate the response of NSC, HPC, and UHPFRC beams with plastic strain contour. NSC flexural member deformed, and spalling damage in the portion was found, which can be seen when strains are stabilized, and contours show significant cracking in NSC and HPC slabs. However, no scabbing, spalling, or peeling of concrete was observed in HPC assembly. Therefore, UHPFRC illustrated considerable strength and energy absorption capacity compared with NSC, and HPC may be conveniently used in blast-resistant structures.

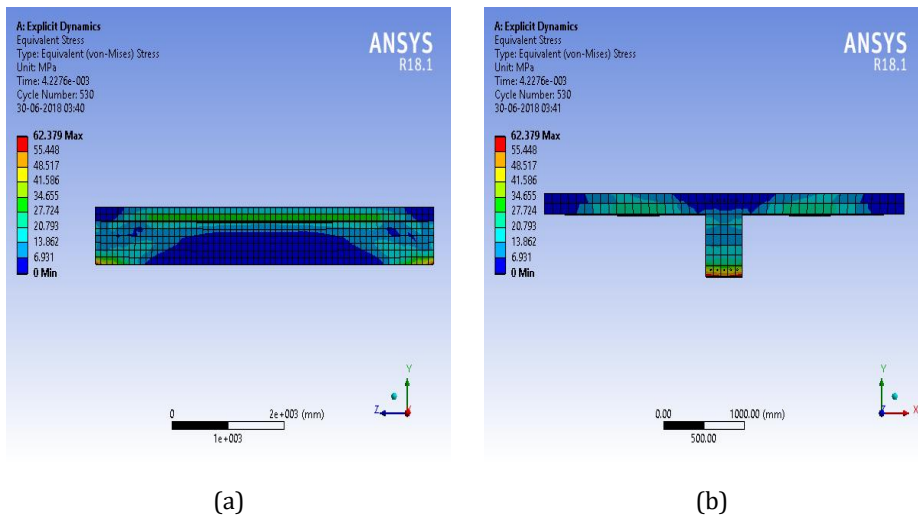
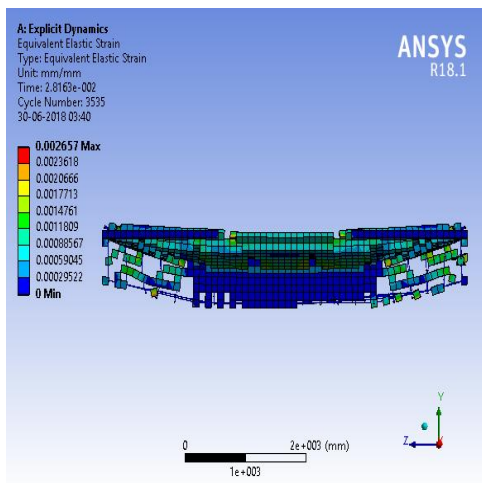
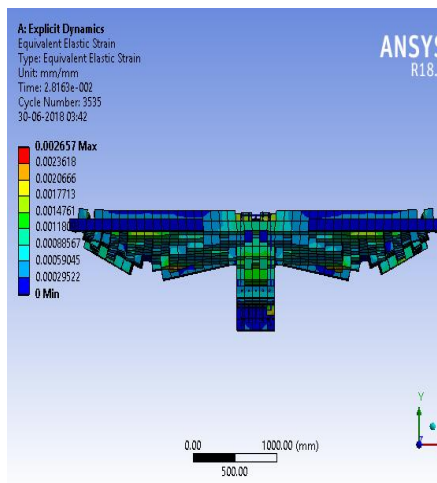


Fig. 15 (a, b) Equivalent stress pattern for NSC

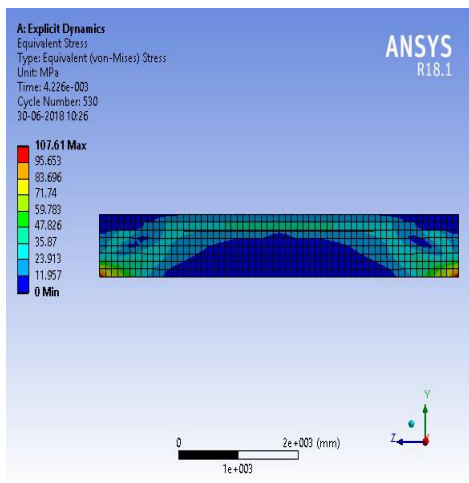


(a)

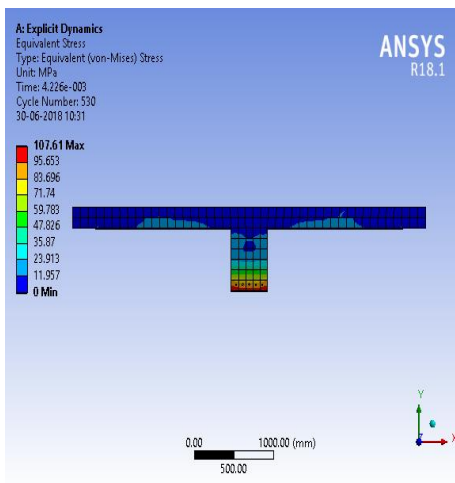


(b)

Fig. 16 (a, b) Equivalent strain pattern for NSC

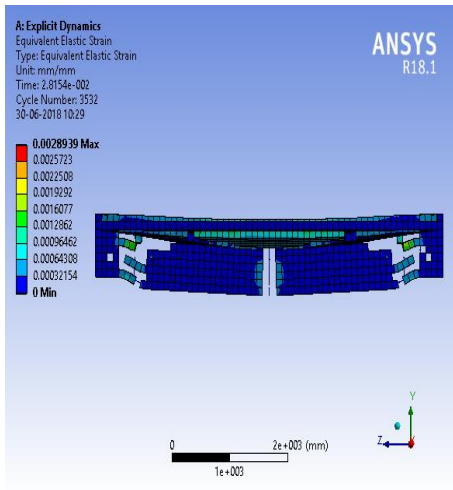


(a)

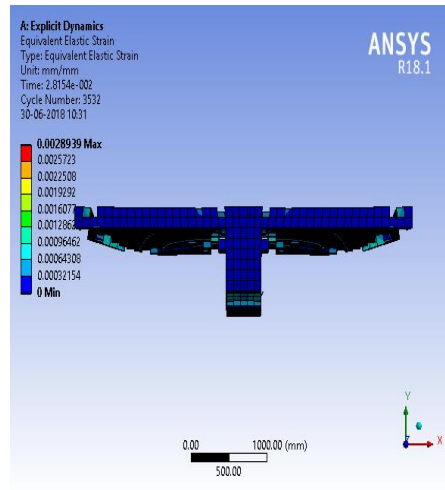


(b)

Fig. 17 (a, b) Equivalent Stress Pattern for HPC

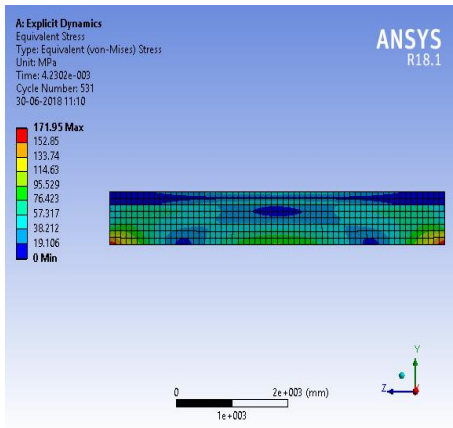


(a)

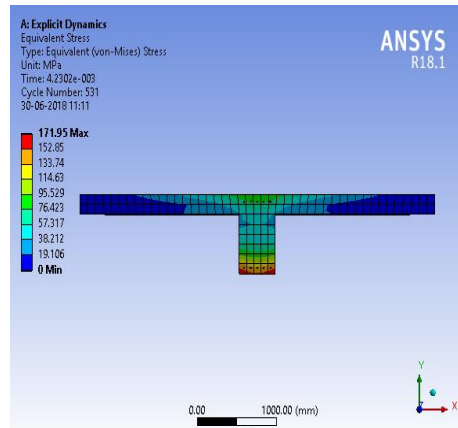


(b)

Fig. 18 (a, b) Equivalent Strain Pattern for HPC



(a)



(b)

Fig. 19 (a, b) Equivalent Stress Pattern for UHPFRC

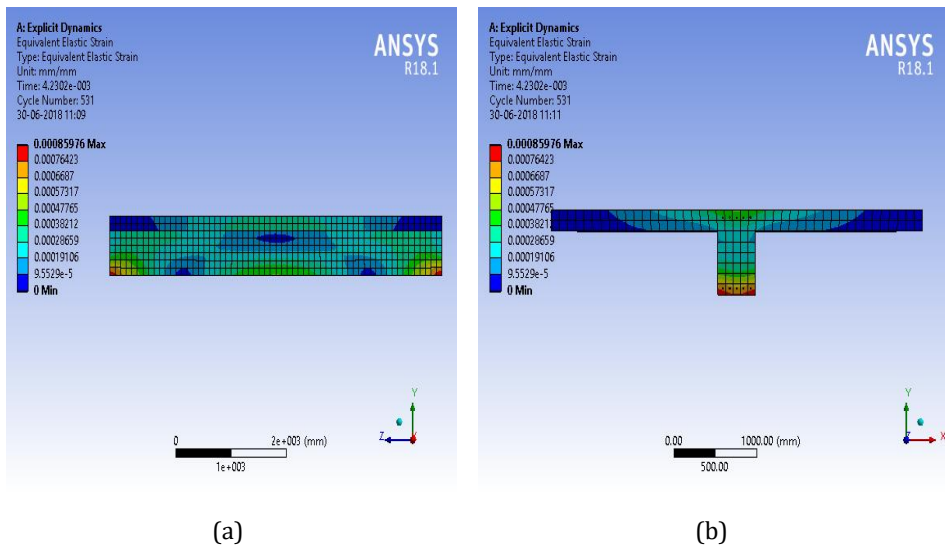


Fig. 20 (a, b) Equivalent Strain Pattern for UHPFRC

6.4 Damage Behaviour

Fig. 21-22 illustrate the damage pattern in NSC and HPC beams under 25 kN of TNT. There is no damage occurs in the UHPFRC slab beam assembly at a load intensity of 25 kN. As explained earlier, concrete crushing, spalling, and peeling is an exceedingly localized phenomenon, and the structure re-establishes its strength in the short period in UHPFRC. High CS associated with significant flexural and shear strength significantly confined damage compared to NSC.

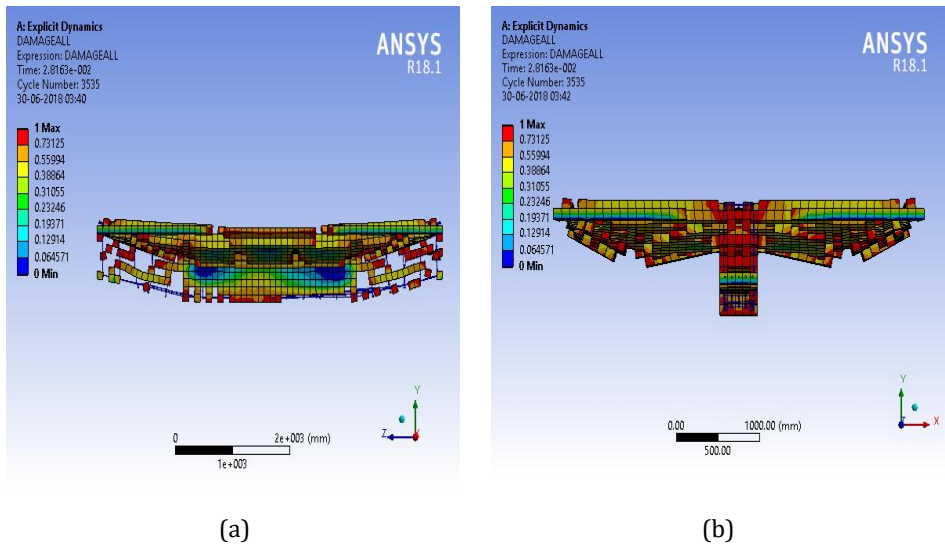


Fig. 21 (a, b) Damage Pattern of NSC

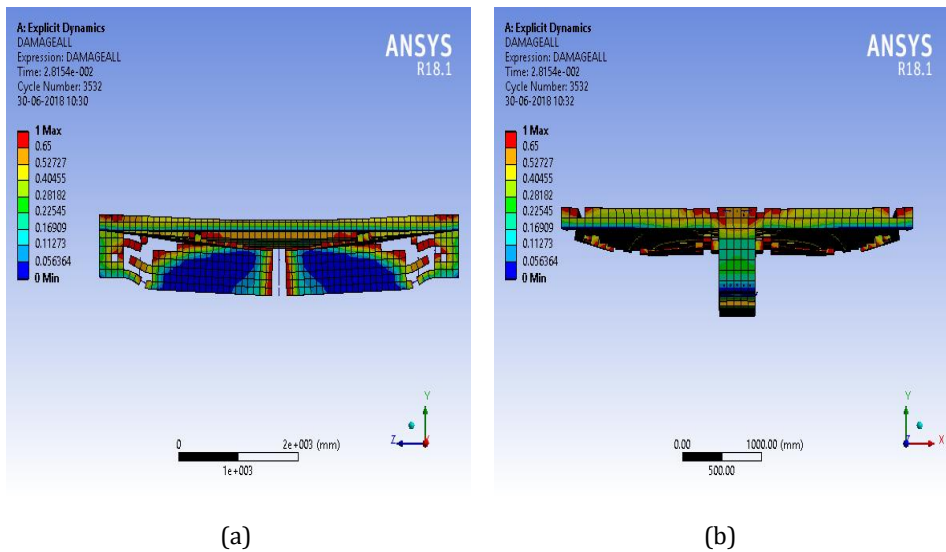


Fig. 22 (a, b) Damage Pattern of HPC

6.5 Comparison of Results

The time history curves of the flexural structural system are plotted for HPC, shown in Fig. 23. It has been observed that the dynamic analysis of the assembly gives a maximum deformation of 1.27 mm and a peak value of 1.81 mm obtained numerically. It has also been seen that higher values demonstrated a plastic deformation in HPC flexural members. Due to the wide-open cracks, the total deformation gradually decreased by 0.19 mm at 10 ms to transfer the stresses in the reinforcing bars. The use of SF reinforcement in the UHPFRC assembly has been found to significantly reduce spall damage in concrete. Therefore, it conclusively stated that the numerical model presented in this research work could reproduce the damage response of NSC, HPC, and UHPFRC assembly under blast loads. UHPFRC produced superior blast resistance capacity compared with NSC and HPC.

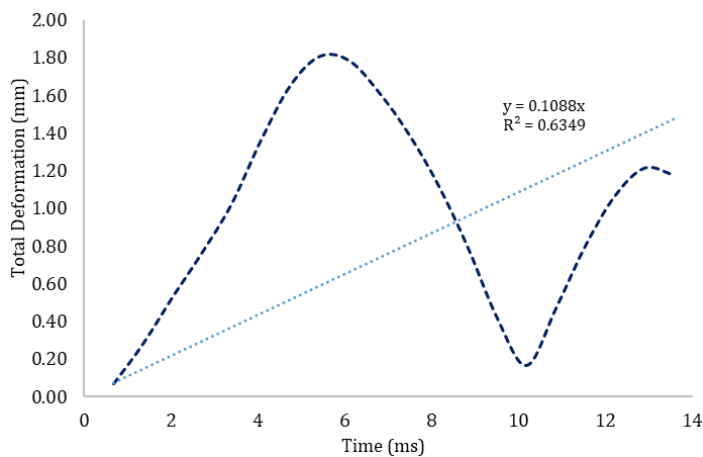


Fig. 23 Total Deformation and Time-History Curve for HPC

The pattern of peak deformation with blast intensity demonstrates that the values in NSC, HPC, and UHPFRC are minimal blast loads of 5 and 10 kN, as shown in Fig. 24. At 15 kN TNT, NSC members showed a significant deformation. At 25 kN intensity, peak deformations in NSC and HPC were increased significantly, and the structure may not survive under the blast load. However, a small deformation was shown by the UHPFRC assembly, which illustrates that the member withstands a higher blast intensity of 25 kN. The load-deformation curve calculated the values of energy absorption capacity, improved strength, stiffness, and ductility. Therefore, the UHPFRC assembly can withstand blast loads of higher intensities without appreciable damage. UHPFRC was also an efficient material that could withstand a blast of large magnitude at a small distance.

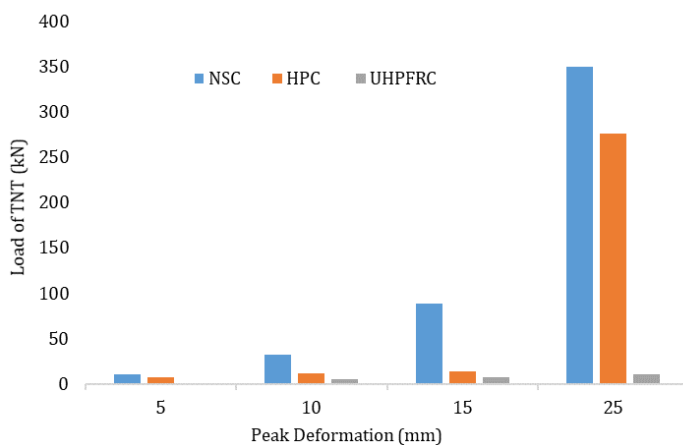


Fig. 24 Load-Deformation behaviour of different strengths of concrete

The comparison of maximum stress with blast intensity for NSC, HPC, and UHPFRC is shown in Fig. 25-26. It illustrates the exciting results at low blast loads and maximum stress developed when the blast intensity increases in the case of NSC and HPC. However, there is no variation in HPC and UHPFRC due to their improved toughness and energy absorption capacity.

At the peak blast intensity of 25 kN, a significant variation was observed for maximum stresses. The values of NSC, HPC, and UHPFRC vary in strength, compactness, and energy absorption capacity. In comparison, maximum strain values on the lower side in UHPFRC compared with NSC and HPC. After validating with UHPFRC, flexural member possesses improved resistance against blast loads of higher magnitude and can be used advantageously for structures of strategic significance near border areas and structures of national importance. Since the numerical model provides an excellent prediction of the damage to the structure, it is always possible to enhance structural performance against blast. Improving the toughness of key elements and increasing SD can further provide occupants with a reasonable chance to escape injury and death.

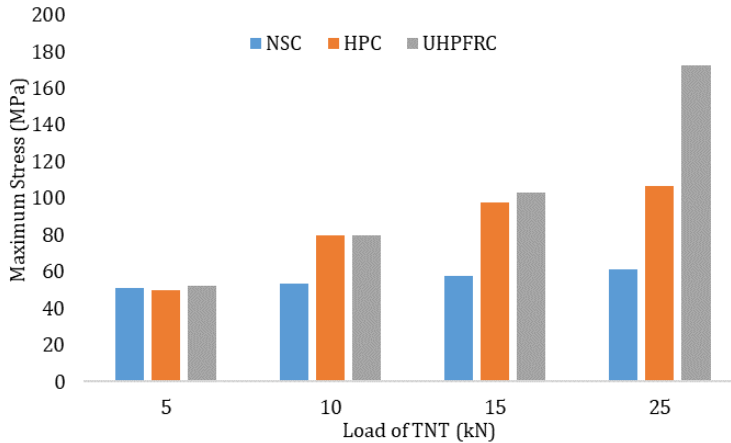


Fig. 25 Maximum Stress Vs. Blast Load Intensity Behaviour for Different Grades of Concrete

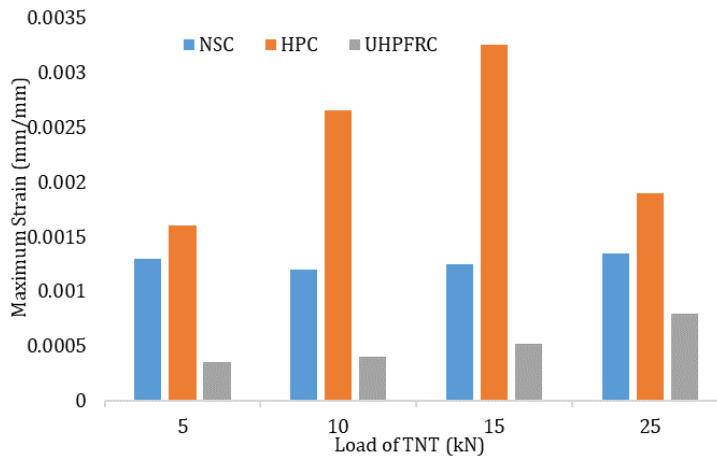


Fig. 26 Maximum Strain Vs. Blast Load Intensity for Different Grades of Concrete

7. Conclusions

The present study demonstrates the performance of NSC, HPC, and UHPFRC flexural assemblies under high strain rate conditions of blast loading. Based on the analysis and detailed investigation, the following conclusions are drawn.

- UHPFRC offers the improved capability to distribute an enormous amount of energy under blast loading compared to NSC and HPC. Hence, UHPFRC can be used to construct blast-resistant structures because of the fact that it has about four times higher force capacity for the same size and reinforcement.
- UHPFRC flexural members demonstrate greater compressive and tensile resistance against extreme conditions like blast, impact loadings.
- Compared with controlled concrete, a significant reduction in total deformation of 22 and 99% have been observed in HPC and UHPFRC.

- NSC members were severely damaged because of the weak bond with steel reinforcement under blast loads, and bond failure was observed between the composite and reinforcement when subjected to a blast load of 25 kN. HPC, however, did not fail due to de-bonding with reinforcement and offered bond resistance more effectively than NSC for more duration. UHPFRC was also capable of surviving the blast load during the entire period of blast and showed no damage.
- The flexural members are designed to resist blast load of 1.315 kN at a charge weight of 5 kN within the elastic-range, and 15 kN in the plastic- range due to HPC and UHPFRC.
- UHPFRC enhances flexural stiffness of structural members significantly thereby decreasing section dimensions, resulting in reduced dead load.
- UHPFRC was also an efficient material that could withstand a blast of large magnitude at a small distance.
- The numerical model presented in this research work could reproduce the damage response of NSC, HPC, and UHPFRC assembly under blast loads. UHPFRC produced superior blast resistance capacity compared with NSC and HPC.

References

- [1] Ngo T, Mendis P, Ramsay J. Blast Loading and Blast Effects on Structures – An Overview, EJSSE Special Issue: Loading on Structures. 2007; 76–91.
- [2] Rizwanullah, Sharma HK. Influence of critical parameters on UHPFRC structural elements subjected to blast loading. SN Applied Science. 2020; 2:486. <https://doi.org/10.1007/s42452-020-2259-5>.
- [3] Büyüköztürk O, Denvid L. High performance concrete: fundamentals and application. Massachusetts Institute of Technology, Cambridge, Massachusetts, US, 2002; 1-20.
- [4] Rizwanullah, Sharma HK, Blast loading effects on UHPFRC structural elements: a review, Innovative Structure Solutions, 2022; 7:341, <https://doi.org/10.1007/s41062-022-00937-2>.
- [5] Larrad FD, Sedran T. Optimization of Ultra high performance concrete by the use of a packing model, Cement and Concrete Research, 1994; 24 (6), 997–1009.
- [6] Feylessoufi A, Crespin M, Dion P, Bergaya F, Van DH, Richard P. Controlled Rate Thermal Treatment of Reactive Powder Concretes, Advanced Cement BASED Materials, 1997; (6): 21–27.
- [7] Fehling E, Schmidt M, Walraven J, Leutbecher T, Fröhlich S. Ultra-High Performance Concrete UHPC. Fundamentals, Design, Examples. First Edition, 2015; 1-188.
- [8] Yi N-H, Kim J-HJ, Han T-S, Cho Y-G, Lee JW. Blast-resistant characteristics of ultra-high strength concrete and reactive powder concrete, Construction and Building Material, 2012;28; 694–707, <https://doi.org/10.1016/j.conbuildmat.2011.09.014>.
- [9] Thomas RJ, Sorensen AD. Review of strain rate effects for UHPC in tension, Construction and Building Materials, 2017;153; 846–856, <https://doi.org/10.1016/j.conbuildmat.2017.07.168>.
- [10] Unified Facilities Criteria (UFC) 3-340-02: Structures to resist the effects of accidental explosions, 2008; Department of the Army, the NAVY and the Air Force, Washington DC, USA, 1-1867.
- [11] Brode HL. Numerical Solutions of Spherical Blast Waves, Journal of Applied Physics, American Institute of Applied Physics, New York, 1955; 26(6), 766–775. <https://doi.org/10.1063/1.1722085>.
- [12] Karlos V, Solomos G. Calculation of blast loads for application to structural components, JRC Technical report, EUR 26456 EN.2013; <https://doi.org/10.2788/61866>.

- [13] Sadovskiy MA. Mechanical effects of air shock waves from explosions according to experiments, 2004; Selected works: Geophysics and physics of explosion, Nauka Press, Moscow.
- [14] Adushkin VV, Korotkov AI. Parameters of a shock wave near to HE charge at explosion in air. PMTF, 1961; 119-123.
- [15] Newmark NM, Hansen RJ. Design of blast resistant structures, shock and vibration handbook, Harris, Crede eds, McGraw-Hill, 1961, New York, USA.
- [16] J. Henrych, and R. Major. The Dynamics of Explosion and Its Use, NUCLEAR TECHNOLOGY, 1979, Elsevier, Amsterdam.
- [17] Held M. Blast Waves in Free Air, Propellants, Explosives Pyrotechnics, 1983; 8 (1), 1-7, <https://doi.org/10.1002/prop.19830080102>.
- [18] Kinney GF, Graham KJ. Explosive Shocks in Air, The Journal of the Acoustical Society of America, Springer-Verlag, Berlin and New York, 1985; 80(2), <https://doi.org/10.1121/1.394030>.
- [19] Mills CA. The design of concrete structure to resist explosions and weapon effects, Proceedings of the 1st International Conference on Concrete and Hazard Protections, 1987; 61-73.
- [20] Hopkins-Brown MA, Bailey A. Chapter 2 (Explosion Effects) Part 1, AASTP-4 Royal Military College of Science, 1998; Cranfield University.
- [21] Low HY, Hao H. Reliability analysis of reinforced concrete slabs under explosive loading, Structural Safety, 2001; 23 (2): 157-178, [https://doi.org/10.1016/S0167-4730\(01\)00011-X](https://doi.org/10.1016/S0167-4730(01)00011-X).
- [22] Gelfand B, Silnikov M, Translation from Russian to English Book, Blast effect caused by Explosions, 2004; DTIC, Document, London, England.
- [23] Wu C, Hao H. Modelling of simultaneous ground shock and air burst pressure on nearby structures from surface explosions, International Journal of Impact Engineering, 2005; 31(6): 699-717, <https://doi.org/10.1016/j.ijimpeng.2004.03.002>.
- [24] Nyström U, Gylltoft K. Numerical studies of the combined effects of blast and fragment loading, International Journal of Impact Engineering, 2009; 36: 995-1005, <https://doi.org/10.1016/j.ijimpeng.2009.02.008>.
- [25] Luccioni BM, Ambrosini RD, Danesi RF. Analysis of building collapse under blast loads, Engineering Structures, 2004; 26: 63-71, <https://doi.org/doi.1016/j.engstruct.2003.08.011>.
- [26] Byfield MP. Behavior and Design of Commercial Multistory Buildings Subjected to Blast, Journal of Performance of Constructed Facilities, 2006; 20(4), 324-329. [https://doi.org/10.1061/\(ASCE\)0887-3828\(2006\)20:4\(324\)](https://doi.org/10.1061/(ASCE)0887-3828(2006)20:4(324)).
- [27] Shi Y, Hao H, Li Z-X. Numerical simulation of blast wave interaction with structure columns, Shock Waves, 2007; 17: 113-133, <https://doi.org/10.1007/s00193-007-0099-5>.
- [28] Kocczaz Z, Sutcu F, Torunbalci N. Architectural and structural design for blast resistant buildings, In: The 14th World Conference on Earthquake Engineering, The 14 World Conference on Earthquake Engineering, October 12-17, 2008, Beijing, China.
- [29] Wu, C, Oehlers DJ, Rebentrost M, Leach J, Whittaker AS. Blast testing of ultra-high performance fibre and FRP-retrofitted concrete slabs, Engineering structures, 2009; 31(9): 2060-2069, <https://doi.org/10.1016/j.engstruct.2009.03.020>.
- [30] Hassan MZ, Guan Z. W, Cantwell, WJ, Langdon, GS, Nurick GN. The influence of core density on the blast resistance of foam-based sandwich structures. International Journal of Impact Engineering, 2012; 50:9-16, <https://dx.doi.org.10.1016/j.ijimpeng.2012.06.009>.
- [31] Shallan O, Eraky A, Sakr T, Emad S. Response of Building Structures to Blast Effects, International Journal of Engineering and Innovative Technology, 2014; 4:167-175.
- [32] Nicolaidis D, Kanellopoulos A., Petrou M, Savva P, Mina A. Development of a new Ultra High Performance Fibre Reinforced Cementitious Composite (UHPFRCC) for impact

- and blast protection of structures, *Construction and Building Materials*, 2015; 95:667-674, <https://dx.doi.org/10.1016/j.conbuildmat.2015.07.136>.
- [33] Kyei C, Braimah A. Effects of transverse reinforcement spacing on the response of reinforced concrete columns subjected to blast loading, *Engineering Structures*, 2017; 142:148–164, <https://doi.org/10.1016/j.engstruct.2017.03.044>.
- [34] Li J, Hao H, Wu C. Numerical study of precast segmental column under blast loads, *Engineering Structures*, 2017; 134:125–137, <https://doi.org/10.1016/j.engstruct.2016.12.028>.
- [35] Yang HW, Guan WB, Lu GY. Experimental and numerical investigations into collapse behavior of hemispherical shells under drop hammer impact. *Thin-Walled Structures*, 2018; 124:48-57, <https://doi.org/10.1016/j.tws.2017.11.034>.
- [36] Turker K, Hasgul U, Birol T, Yavas A, Yazici H. Hybrid fiber use on flexural behavior of ultra high performance fiber reinforced concrete beams, *Composite Structures*, 2019; 229:111400, <https://doi.org/10.1016/j.compstruct.2019.111400>.
- [37] Lee J-Y, Aoude H, Yoon Y-S, Mitchell D. Impact and blast behavior of seismically-detailed RC and UHPFRC-Strengthened columns, *International Journal of Impact Engineering*, 2020; 143:103628, <https://doi.org/10.1016/j.ijimpeng.2020.103628>.
- [38] Castedo R, Santos AP, Alañón A, Reifarth C, Chiquito M, López LM, Martínez-Almajano S, Pérez-Caldentey A. Numerical study and experimental tests on full-scale RC slabs under close-in explosions, *Engineering Structures*, 2021; 231:111774, <https://doi.org/10.1016/j.engstruct.2020.111774>.
- [39] Kadhim MMA, Jawdhari A, Peiris A. Development of hybrid UHPC-NC beams: A numerical study, *Engineering Structures*, 2021; 233:111893, <https://doi.org/10.1016/j.engstruct.2021.111893>.
- [40] Mahmud GH, Hassan AMT, Jones SW, Schleyer GK. Experimental and numerical studies of ultra high performance fibre reinforced concrete (UHPFRC) two-way slabs, *Structures*, 2012; 29:1763–1778, <https://doi.org/10.1016/j.istruc.2020.12.053>.
- [41] Mandal J, Goel MD, Agarwal AK. Surface and Buried Explosions: An Explorative Review with Recent Advances, *Archives of Computational Methods in Engineering*, 2021; <https://doi.org/10.1007/s11831-021-09553-2>.
- [42] Anas SM, Mehtab Alam, Mohammad Umair. Reinforced cement concrete (RCC) shelter and prediction of its blast loads capacity. *Materials Today: Proceedings*, 2022; <https://doi.org/10.1016/j.matpr.2022.09.125>.
- [43] Yan J, Liu Y, Bai F, Ni X, Xu Y, Yan Z, Huang F. Dynamic response of GFRP-reinforced UHPC beams under close-in blast loading. *Materials & Design*, 2022; 223, 111140, <https://doi.org/10.1016/j.matdes.2022.111140>.
- [44] Ma LL, Wu H, Fang Q. A unified performance-based blast-resistant design approach for RC beams/columns. *International Journal of Impact Engineering*, 2023; 173:104459, <https://doi.org/10.1016/j.ijimpeng.2022.104459>.
- [45] K. Peter. ANSYS Theory Reference Release 5.6, 1994.